Scientific Research Publishing

Computational Chemistry, 2023, 11, 53-66
https://www.scirp.org/journal/cc
ISSN Online: 2332-5984
ISSN Print: 2332-5968

Functionality of Covalent Organic Framework (COF) in Gas Storage Application: First Principal Study

Mashael Alharbi, Raghad Aljohani, Raghad Alzahrani, Yara Alsufyani, Nuha Alsumani

Faculty of Science, Chemistry Department, King Abdulaziz University, Jeddah, Saudi Arabia
Email: nwazzan@kau.edu.sa

How to cite this paper: Alharbi, M., Aljohani, R., Alzahrani, R., Alsufyani, Y. and Alsumani, N. (2023) Functionality of Covalent Organic Framework (COF) in Gas Storage Application: First Principal Study. *Computational Chemistry*, **11**, 53-66.
https://doi.org/10.4236/cc.2023.113004

Received: May 7, 2023
Accepted: May 28, 2023
Published: May 31, 2023

Abstract

Industrial growth in recent years led to air pollution and an increase in concentration of hazardous gases such as O_3 and NO. Developing new materials is important to detect and reduce air pollutants. While catalytic decomposition and zeolites are traditional ways used to reduce the amount of these gases. We need to develop and explore new promising materials. Covalent organic framework (COF) has become an attractive platform for researcher due to its extended robust covalent bonds, porosity, and crystallinity. In this study, first principal calculations were performed for gases adsorption using COFs containing nitrogen and π-bonds. Different building blocks (BBs) and linkers (LINKs/LINK1 & LINK2) were investigated by means of density functional theory (DFT) calculations with B3LYP and 3-21G basis sets to calculate the binding energies of gases @COF systems. Electrostatic potential maps (ESPM), Mulliken charges and non-covalent interaction (NCI) are used to understand the type of interactions between gas and COFs fragments. O_3 was found to bind strongly with COF system in comparison with NO which could make COF a useful selective material for mixed gases environment for sensing and removal application.

Keywords

Covalent Organic Framework (COF), Ozonestorage, Nitric Oxide Storage, First Principal Study, Binding Energies, Non-Covalent Interaction (NCI) Analysis, Effect of π-Linkers and Building Blocks

1. Introduction

Human activity is altering global environmental conditions, affecting global biogeochemical flows (e.g., nitrogen, ozone) thus the quality of the air, water, and

soil, along with habitat loss and climate change [1]. Ground-level ozone is a colourless and highly irritating gas that forms above the earth's surface. It is referred to as "secondary" pollutant because it is formed when two primary pollutants react in sunlight and air. These two primary pollutants are nitrogen oxides (NOx) and volatile organic compounds (VOCs) [2]. NOx and VOCs are produced by both natural and human activities. Approximately 95% of NOx emissions from human activity are caused by the combustion of coal, gasoline, and oil in automobiles, homes, industries, and power plants [3]. Tropospheric ozone is a significant greenhouse gas that is also phytotoxic. Ozone levels have increased by 35% since the beginning of the industrial period [4]. Increased ozone concentrations can be harmful in terms of adverse effects on human health [5] besides its ability to inhibit photosynthesis and plant growth, affecting vegetation and crops [6]. The current Occupational Safety and Health Administration (OSHA) Air Quality Guidelines for workplace ambient ozone recommend a limit of 200 μgm^{-3} (≈ 100 ppb). Working in an environment that exceeds the limit may pose health risks to humans [7].

Nitric oxide (NO) is a colourless, odourless gas that is soluble in aqueous and organic solvents and its decomposition product contains numerous of unstable nitroso and nitro compounds [8]. NO is a reactive gas that influences ozone production and destruction thus plays an important role in atmospheric chemistry. Moreover, NO contributes to acid rain formation through its oxidation products. Anthropogenic emissions (from the combustion of fossil fuels) and biogenic emissions from soils are the two major sources of NO in the atmosphere [9].

Thus, developing new materials to detect and reduce ozone and nitric oxide pollutants is considered of a significant and urgent demand. The dominant approaches for ozone removal are based on traditional activated carbon adsorption, chemical absorption, and catalytic decomposition methods [7]. While ion exchanged zeolites are well known for their efficient catalytic NO conversion [10]. Currently, there is still lacking advanced materials that can be applied for sensing and removal of air pollutants like ozone and nitric oxide [7]. Covalent organic frameworks (COFs) are covalent porous crystalline polymers that allow for the intricate integration of organic building components into an organized structure with atomic precision to construct predesigned skeletons and nanopores [11]. They have recently become an attractive molecular platform for gas storage [12], catalysis [13], drug delivery [14], sensing [15], semiconductors (p and n-type) [16], electrodes for supercapacitors in lithium batteries [17] mass transport [18], stationary phase in chromatographic columns [19], and optoelectronic applications [20]. The synthesis of various covalent organic frameworks (COFs) and metal organic frameworks (MOFs), in which the pore shape, size, and pore's functionality can be designed for specific applications, has been made possible by reticular chemistry, which is a branch of chemistry that concern of linking well-defined molecular building blocks by robust bonds to form extended crystalline frameworks [21]. Three crucial factors in the reticular de-

sign and synthesis of COFs involve the reversibility of dynamic covalent reactions, the variety of building blocks, and geometry retention [11].

Organic linkers are used to construct covalent organic frameworks via slightly reversible condensation reactions. While the covalent bonds formed in the frameworks allow for high thermal stability, the reversible nature of the relevant coupling reactions allows for the formation of a crystalline structure rather than an amorphouspolymer enables for error correction and network rearrangement via cleavage and reformation of connections within the lattice [22].

Omar Yaghi and his group reported the first series of 2D COFs in 2005. Successful design and synthesis of COFs was done by condensation reactions of phenyl diboronic acid ($C_6H_4[B(OH)_2]_2$) resulting in extended framework, COF-1, **Figure 1**. Strong bonds between B, C, and O atoms hold the crystal structure together, generating rigid porous architectures with pores that vary in size from 7 to 27 Å.COF-1 exhibit high thermal stability (to temperatures reaching 500˚C - 600˚C), permanent porosity, and high surface areas (711 m^2/g) [23]. Followed by 3D COFs synthesis by Yaghi and colleagues in 2007 as crystalline solids by co-condensing triangular 2, 3, 6, 7, 10, 11-hexahydroxytriphenylene with tetrahedral tetra (4dihydroxyborylphenyl) methane or tetra (4-dihydroxyborylphenyl) silane. These materials have high thermal stabilities (400˚C - 500˚C), high surface areas (3472 and 4210 m^2/g for COF-102 and COF-103, respectively), and extremely low (0.17 g/cm^3) densities since they are entirely made of strong covalent bonds (C–C, C–O, C–B, and C–O) [24].

Compared with inorganic porous crystalline materials such as zeolites and hybrid inorganic-organic metal organic frameworks (MOFs), COF can effectively avoid the connection of metal nodes in the framework that may exhibit certain toxicity and have a lower skeleton density [25]. In contrast of conventional linear polymers, COF allow for positional control of their building units in two and three dimensions. This control allows for the synthesis of structures with high regularity as well as the fine-tuning of the network's chemical and physical properties [22] Evolution of crystalline porous materials shows in **Figure 2**.

The geometry and connectivity of the linkers determine the geometry of the framework in a COF lattice as shown in **Figure 3**. For example, trigonal planar linkers can co-condense to form sheets with hexagonal pores, whereas tetragonal linkers co-condense to form tetragonal pores when combined with linear building blocks. COFs created from stacked 2D layers are commonly referred to as 2D COFs, whereas 3D COFs are created from building blocks with three-dimensional connectivity, resulting in the formation of a 3D net [22].

Research have found that different gases could be adsorbed on different types of COF. Dash (2018) investigated the molecular-scale physical binding phenomena that take place when CO_2 and N_2 gas molecules interact with the COF's building blocks from binding energy (BE) calculations using DFT. Dash noticed that CO_2 has higher BE near the triazine moiety whereas, in the case of N_2, the BE near nitrogen-containing rings were calculated to be low. This CO_2-philicity

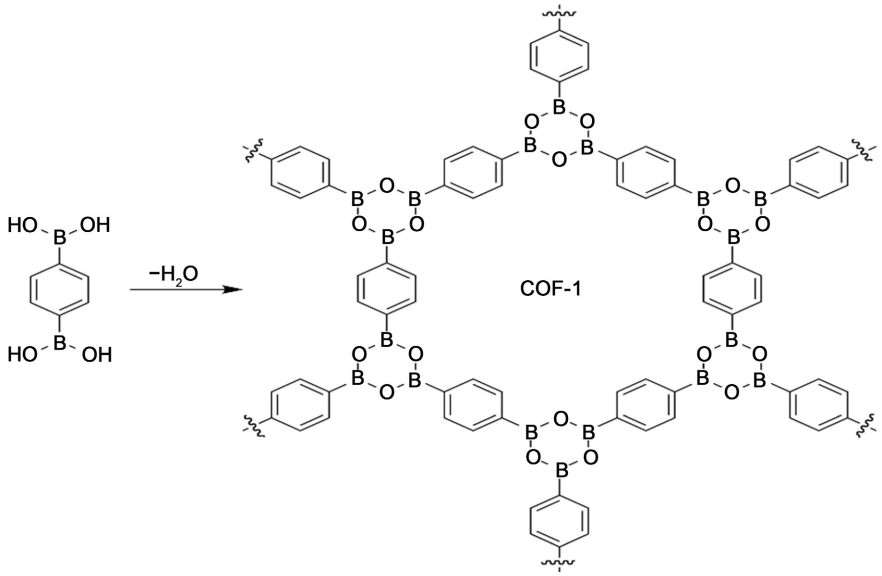

Figure 1. Phenyldiboronic acid condenses to form COF-1, which is composed of phenyl rings connected by boroxine rings [23].

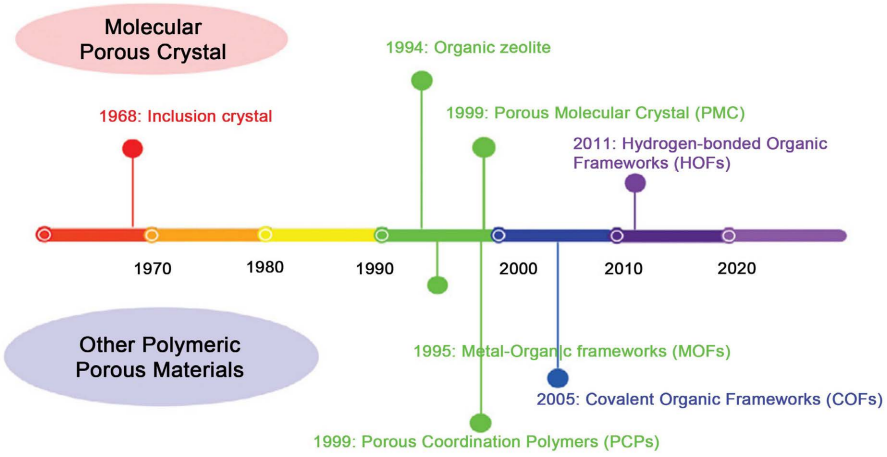

Figure 2. Representation of the development of crystalline porous materials [25].

and N_2 phobicity property makes it obvious that COF could be used for both CO_2 uptake and CO_2/N_2 selectivity [26]. Imine-based COFs were developed as smart ozone-responsive materials by Yan *et al.* in 2021 to detect and remove ozone through treatment with both wet and dry ozone. If moisture is present, imine groups prefer to bind with water molecules to help facilitate the protonation of C=N to $C=NH^+$ groups, which causes the visible colour change; whereas if moisture is not present, ozonenucleophilically attack imine groups and converted to nitro, aldehyde, and carboxylate moieties proving the quick optical responses and the excellent performance of the imine-based COFs. These findings continue to build knowledge and capability of such new emerging type of material in gas adsorption application [7].

In this work, DFT methods were used to examine N-containing organic framework (COF) material for ozone and nitric oxide gases adsorption/sensing

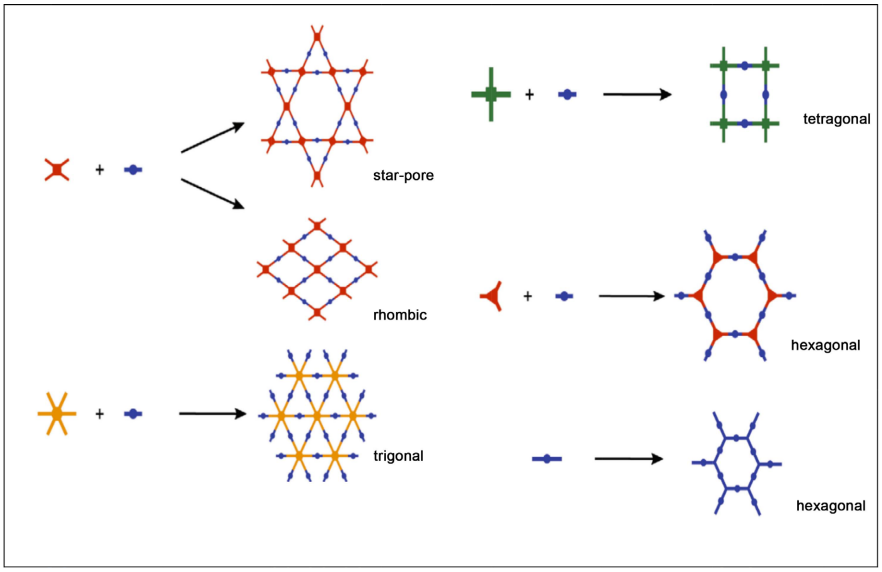

Figure 3. Depicts an overview of common 2D geometries recognized in COFs [22].

application. In this study we used two building blocks/knots abbreviated as BB1 = 2*H-imidazole*, BB2 = (E)-1,2-di(2H-imidazol-2-yl)diazene connected with either linker1 = 4,4'-di(2H-imidazol-2-yl)-[1,1'-biphenyl]-2-aminesubstituted with -NH_2 or linker2 = 2,2'-(2-nitro-[1,1'-biphenyl]-4,4'-diyl) bis(2H-imidazole) substituted with -NO_2 as demonstrated in **Figure 4**. The effect of nature of BBs and LINKs substituted with electron donating/withdrawing groups on the interactions with gases have been illustrated using binding energies, interacting distances, non-covalent interaction (NCI), electrostatic potential surfaces maps (EPSMs) and Mulliken charges (**Figure 5**).

2. Computational Methods

Calculations were performed using first principal methods based on DFT implemented in the Gaussian 09 package [27]. Geometry optimizations of free gasses, free building blocks and π-linkers, and for adsorbed systems of gasses were performed at Becke-three-parameter Lee-Yang-Parr (B3LYP) functional [28] with 3 - 21 G basis set [29]. Frequency calculations were performed to ensure that the optimized geometries are minima points in their potential energy surfaces. The binding energy (BE) between the COF model and Ozone O_3 or Nitric oxide NO was evaluated for geometries optimized using Equation (1). Equation (1) below illustrates the calculation of the BE of gas molecule with N-containing COF model system.

$$\Delta E_{BE} = E_{O_3/NO@COF} - E_{O_3/NO} - E_{COF} \quad (1)$$

where $E_{O_3/NO}$, E_{COF}, $E_{O_3/NO@COF}$ stand for the energies of O_3 or NO molecule, energies of covalent organic framework model system and total energy of the O_3/NO adsorbed-on COF, respectively. Gauss view used for visualization. Multiwfn [30], VMD [31] and Gnup lotused to get NCI plots.

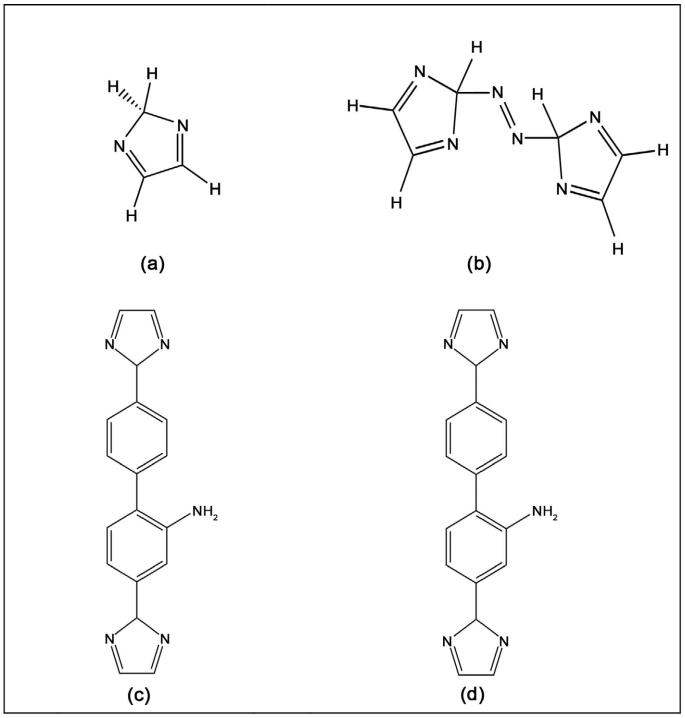

Figure 4. N-containing building block for COFs material. (a) BB1 = 2H-imidazole. (b) BB2 = (E)-1,2-di(2H-imidazol-2-yl)diazene (c) Linker1 = 4,4'-di(2H-imidazol-2-yl)-[1,1'-biphenyl]-2-amine. (d) Linker2 = 2,2'-(2-nitro-[1,1'-biphenyl]-4,4'-diyl) bis(2H-imidazole).

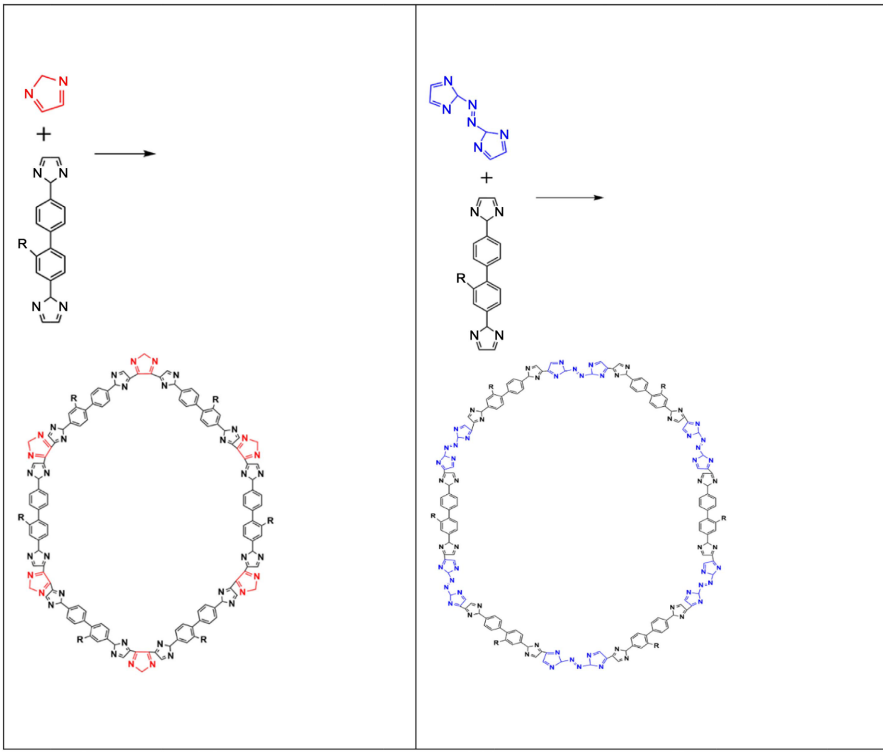

Figure 5. Covalent organic framework (COF) material where R group is either -NH_2 or -NO_2 groups.

3. Results and Discussion

3.1. Bindings Energies

The two gas molecules were placed in the same position with respect to BBs and LINKs. In the case of BBs, O_3 and NO gases were placed close to the nitrogen atom while in the case of LINKs, gases were placed near the substituent groups. Table 1 lists the binding energies and interacting distances of the eight COF systems. BEs were calculated for BB1 and BB2 as shown in Table 1. In BB1 systems, the BEs for O_3@BB1 and NO@BB1 were calculated to be −7.474 and −3.771 kcal/mol, respectively. While the BEs of BB2 with O_3 and NO is as follows, NO@BB2 is −25.745 kcal/mol and for O_3@BB2 is −34.374 kcal/mol, which gives an indication that BB2 is better for gas adsorption than BB1. Moreover, the value of BEs calculated for NO in both BB1 and BB2 is much lower compared to value of O_3 gas proving that O_3 binds more strongly than NO gas.

Different substituted groups in the π-linker and its effect on the binding energy has been investigated, LINK1 substituted with -NH2 group as an electron donating group. On the other hand, LINK2 substituted with an electron withdrawing group (-NO_2). For Link1 systems, the BE of NO@LINK1 is −4.886 kcal/mol and for O3@LINK1 is−14.338 kcal/mol. Likewise the BEs for LINK2 were −4.705 and −11.520 kcal/mol for NO@LINK2and O_3@LINK2, respectively. LINK1 binds the O_3 molecule more efficiently than LINK2, since the BE difference is 2.82 kcal/mol. We noticed that the BE values of LINK1 and LINK2 with NO were significantly lower than those of O_3. The concluded result is that ozone binds strongly with N-containing organic molecules such BB1, BB2, LINK1 and LINK2 compared to NO gas, indicating that they could be more efficient sensors for O_3 than NO gas.

Interacting distances represented the distances between the closest atoms of the two interacting monomers in COF system (gas + COF). Interacting distances are short less than 2.843 Å and ranging from 1.850 to 2.843 Å, the sort interacting distances (less 3 Å) indicating a strong interaction between monomers. We can notice that the smallest distance between H-O (hydrogen bond) in O_3@BB2 system combined the largest binding energy (−34.374 kcal/mol). Another notice is that NO@BB2 system has the second largest BE (−25.745 kcal/mol), and more atoms are interacting with each other.

3.2. Electrostatic Potential Surface Maps (EPSMs)

We studied electrostatic potential surface maps (EPSMs) of the gas molecules involved in interactions to explain their interactions with the nitrogen-containing COF model system. Which shows electrostatics potential regions as well as molecular size and shape is a powerful tool to understand the interaction between gas molecules and COF. Figure 6 shows ESPMs of O_3 and NO calculated at B3LYP and 3 - 21 G level theory. The areas with the highest negative electrostatic potential are emphasised in red (electron rich) regions, while the areas with the highest positive electrostatic potential are indicated in blue colour (electron poor) regions.

Table 1. Binding energies and interacting distances of the investigated eight COF systems.

System	BE (a.u.)	BE (kcal/mol)	Interacting distances (Å)
O_3@BB1	−0.011910	−7.474	N…O 2.217 H…O 2.062
NO@BB1	−0.006009	−3.771	O…H 2.253
O_3@BB2	−0.054780	−34.374	N…O 2.173 H…O 1.850
NO@BB2	−0.041028	−25.745	N…N 2.595 N…H 2.741 O…H 2.294
O_3@Linker1	−0.022849	−14.338	H…O 2.241 N…O 2.471
NO@Linker1	−0.007787	−4.886	O…H 2.118 N…H 2.843
O_3@Linker2	−0.018359	−11.520	N…O 2.787 H…O 2.508
NO@Linker2	−0.007498	−4.705	N…O 2.504

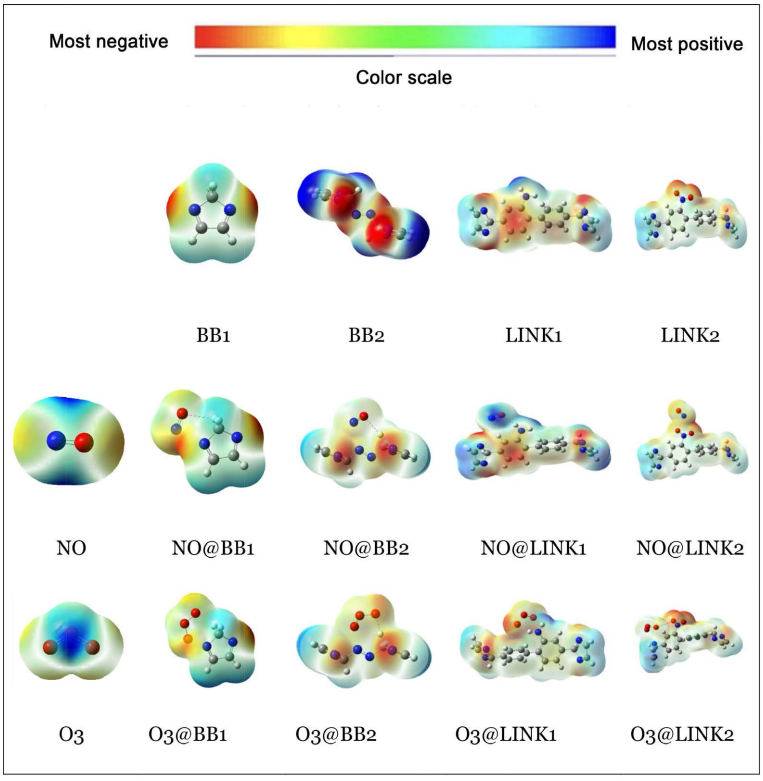

Figure 6. EPSMs of investigated gases, COFs, and gases@COF.

The positive charged region is situated near the carbon atoms in BB1 molecule indicated as blue colour and negative-charged regions indicated in red colour are close to nitrogen atoms. The oxygen atom of NO is attracted to hydrogen atom

of BB1. Similar behaviour between the O of O_3 gas and H of BB1. Repulsion shows in red between two nitrogen atoms of NO and BB1. Thus, we can notice that ozone is more attracted than nitrogen oxide. BB2 provides two rich electron sites. Both nitric oxide and ozone oxygen show hydrogen bonding with the hydrogen of the BB2. Therefore, the formation of H-bonding results in strong interactions between the two gas molecules and BBs.

Linker 1 has (-NH2) as a substituted group on the benzene ring, this substituted effect increase the election density on the benzene because of its electron donating nature. In the case of nitric oxide on Linker1, we can notice blue spot. On the contrary of ozone, there is a slightly red spot between the gas and the adsorbent molecule. NO_2, known as electron-withdrawing group substituted on the benzene ring. As a result -NO_2 pull the electron density from the benzene ring. Ozone shows repulsion force with NO_2 group. While NO appears redder due to attractive with the oxygen molecules in function group that liked in LINK2.

3.3. Mulliken Charges

Table 2 lists the total Mulliken charges on gas molecule before and after binding to COF system, and Figure 7 shows the Mulliken charges distribution on isolated and adsorbed systems. The total charges of gas molecules changed from 0.00 to negative values, indicating intermolecular charge has been transferred between the two interacting monomers. The negative values on gas molecules indicating that the direction of charge transfer is from COF monomer to the gas molecule. The negative charges ranging from −0.020 to −0.267 e. O_3 gas molecule has larger value of total Mulliken charge in all its binding systems compared to NO gas molecule, for example, the charge on O_3 in BB1 COF system equals −0.094 e while the charge on NO molecule in the same COF system is only −0.028 e. This may explain the higher binding of O_3 in COF systems in comparison to NO (larger intermolecular charge transfer is combined with stronger binding and thus larger BE). The exception is O_3@LINK2 where no charge transfer is detected. Since, at the beginning of the optimization process, the O_3 molecule was positioned at the top of the NO_2 substituent on LINK2 and due to the optimization, it orients itself a way from this substituent due to the electrostatic repulsion. Thus, we can attribute the absence of intramolecular charge transfer in this COF system to this type of repulsion.

3.4. Non-Covalent Interaction (NCI)

The reduced density gradient (RDG) method is useful for analysing non-covalent interactions such as hydrogen bonds, Van-der-Waals forces, and steric repulsion. Non-covalent interactions between molecules can be illustrated using scatter plots and non-covalent interaction (NCI) plots. RDG is plotted against electron density multiplied by the sign of the second eigenvalue sign $(\lambda_2)\rho$ in this method [32] Both inter- and intra-molecular weak interactions can be seen

Table 2. Total Mulliken charges (in e) on gas molecule before and after binding to COF system.

System	Before binding	After binding
O3@BB1	0.001	−0.094
NO@BB1	0.00	−0.028
O3@BB2	0.001	−0.165
NO@BB2	0.00	−0.020
O3@Linker1	0.001	−0.267
NO@Linker1	0.00	−0.056
O3@Linker2	0.001	0.000
NO@Linker2	0.00	−0.044

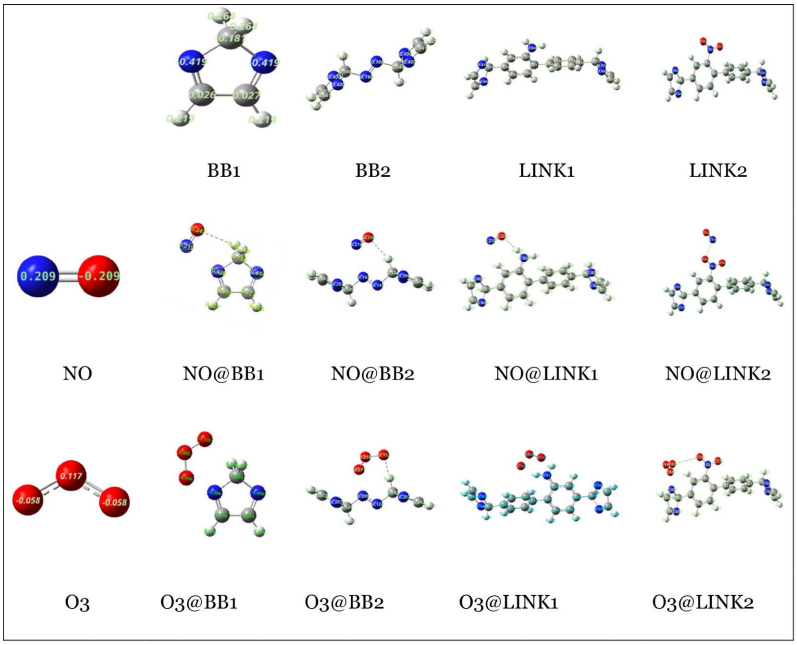

Figure 7. Mulliken charges of investigated gases, COFs, and gases@COF.

in **Figure 8**. RDG scattered points indicate H-bonding interactions on the negative scale (blue colour), and the spikes (green colour) and positive scale of sign $(\lambda_2)\rho$ represent van der Waals interactions and steric repulsions, respectively.

From the above results, we can attribute the stronger interaction between O_3@BB1 and O_3@BB2 to the formation of H-bonds between the O of ozone with the H atom imidazole. While in the case of NO gas, such H-bonds were completely absent since NO gas during the optimization process reorient itself away from H of imidazole. On the other hands, the interaction of O_3 and NO gases with LINK1 and LINK2 is predominated by the week Van der Walls forces. However, a H-bond is formed in the case of O_3/LINK1 which results in higher BE (−14.338 kcal/mol).

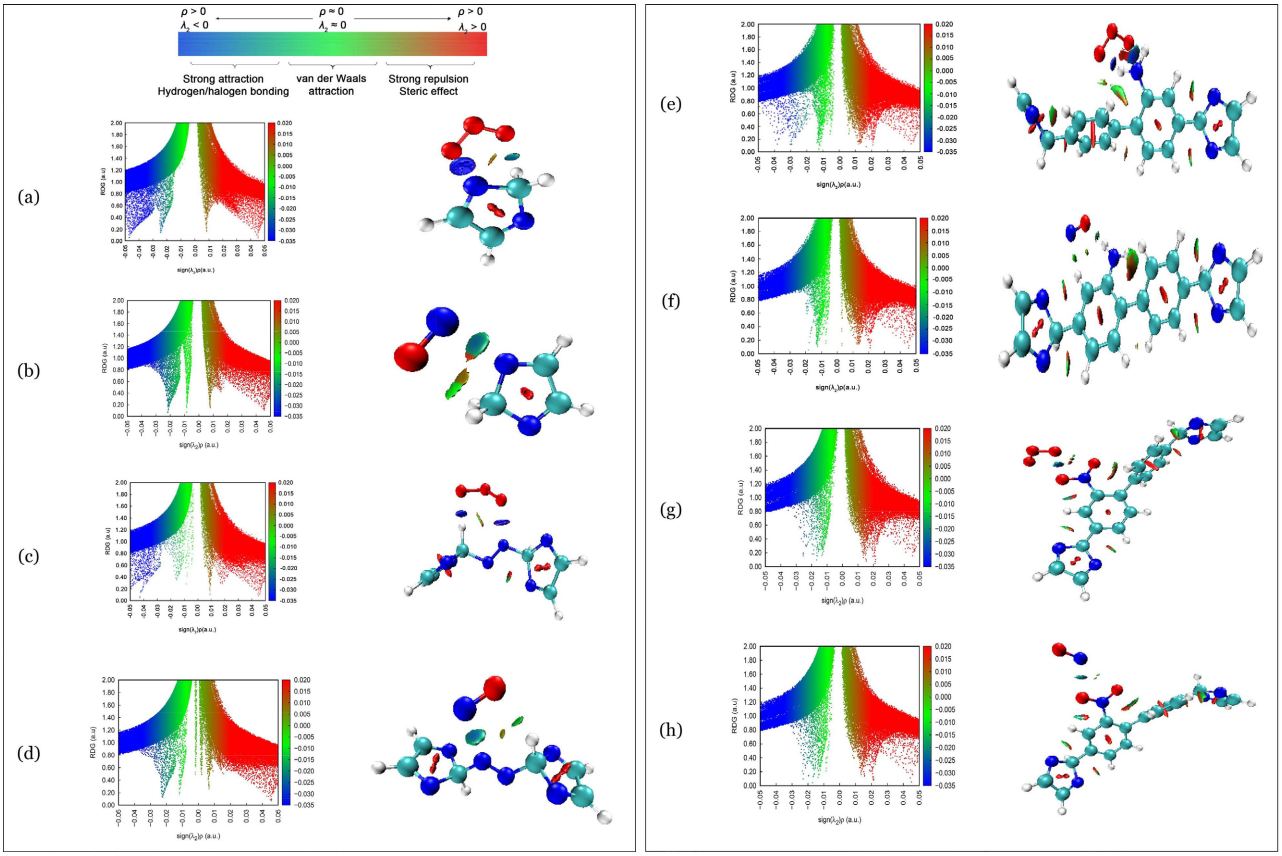

Figure 8. RDG scatter plots (left) and non-covalent interactions (NCI) plots (right) of (a) BB1-O_3, (b) BB1-NO, (c) BB2-O_3, (d) BB2-NO, (e) Linker1-O_3, (f) Linker1-NO, (g) Linker2-O_3 and (h) Linker2-NO. The isosurfaces are coloured according to the values of sign $(\lambda_2)\rho$ (a.u.), from −0.035 to 0.02 a.u. Colour indication: blue represents strong attractive interactions, green indicates van der Waals interactions and red indicates repulsive/steric interactions.

4. Conclusions

In summary, the two gas molecules were placed in the same position relative to the BBs and LINKs, and their binding calculations in the gas phase were performed, in which the B3LYP and 3 - 21 G level of theory was used to calculate the binding energy, interacting distances, Mulliken charges, EPSM, and NCI plots. Conclusions can be drawn as follows:

1) The BEs values of BBs and LINKs with gases (O_3, NO) result that O_3 has higher BEs compared with NOgas, indicating that N-containing COF has stronger ability to bind with O_3 gas.

2) O_3/NO@BB2 shows higher BE values compared to all other systems. Since, O_3@BB2 system has the highest BE (−34.374 kcal/mol) and NO@BB2 system has the second highest value of BE (−25.745 kcal/mol).

3) LINK1 binds the O_3 molecule more efficiently than LINK2, with a BE difference of 2.82 kcal/mol. While, NO@LINK1/LINK2 systems have significantly lower BEs compared to those of O_3@LINK1/LINK2 systems.

4) Mulliken charges showed the magnitude and direction of intermolecular charge transfer between BB/LINK and gases. The total Mulliken charges on gas

molecule before and after the adsorption are all negative (except O_3@LINK2, no charge has been transferred) indicating that the charge is transferred from BB/LINK to the gas molecule.

5) The largest and lowest charge transferred were found to be −0.267e in O_3@LINK1 and −0.020e in NO@BB2, respectively. As a result, we discovered that ozone had a better affinity with BBs and LINKs than nitrogen oxide.

6) NCI plots explained the higher BEs of O_3@BB1/BB2 compared to NO@BB1/BB2 since O_3 has strong hydrogen bonds interaction with BBs.

7) The interaction of O_3 and NO gases with LINK1 and LINK2 is predominated by the week van der walls forces.

8) A H-bond is formed in the case of O_3/LINK1 which results in higher BE (−14.338 kcal/mol) compared to those of NO@LINK1/LINK2 and to that of O_3@LINK2 (BEs ranging from −4.705 to −11.520 kcal/mol).

To conclude, O_3 was found to bind more strongly with our suggested COF system than NO that could nitrogen containing COF a useful selective material for mixed gases environment in sensing and removal application. The exploration of new building blocks for COFs will open new horizons to develop new skeletons, pores, and functions that have outstanding applications in our life.

Acknowledgment

We conducted this research as part of our bachelor's graduation project, as a result, we are grateful for the help and guidance provided throughout this research by the department of Chemistry at King Abdulaziz University, as well as Prof. Nuha Wazzan, the supervisor of our bachelor's graduation project

Conflicts of Interest

The authors declare no conflicts of interest regarding the publication of this paper.

References

[1] Rollin, O., *et al.* (2022) Effects of Ozone Air Pollution on Crop Pollinators and Pollination. *Global Environmental Change*, **75**, Article ID: 102529. https://doi.org/10.1016/j.gloenvcha.2022.102529

[2] Bell, M.L., Zanobetti, A. and Dominici, F. (2014) Who Is More Affected by Ozone Pollution? A Systematic Review and Meta-Analysis. *American Journal of Epidemiology*, **180**, 15-28. https://doi.org/10.1093/aje/kwu115

[3] Zulkifli, M.F.H., *et al.* (2022) Volatile Organic Compounds and Their Contribution to Ground-Level Ozone Formation in a Tropical Urban Environment. *Chemosphere*, **302**, Article ID: 134852. https://doi.org/10.1016/j.chemosphere.2022.134852

[4] Proietti, C., Fornasier, M.F., Sicard, P., Anav, A., Paoletti, E. and De Marco, A. (2021) Trends in Tropospheric Ozone Concentrations and Forest Impact Metrics in Europe over the Time Period 2000-2014. *Journal of Forestry Research* (*Harbin*), **32**, 543-551. https://doi.org/10.1007/s11676-020-01226-3

[5] Liu, H., *et al.* (2018) Ground-Level Ozone Pollution and Its Health Impacts in China. *Atmospheric Environment*, **173**, 223-230.

https://doi.org/10.1016/j.atmosenv.2017.11.014

[6] Tjoelker, M.G. and Luxmoore, R.J. (1991) Soil Nitrogen and Chronic Ozone Stress Influence Physiology, Growth and Nutrient Status of *Pinus taeda* L. and *Liriodendron tulipifera* L. Seedlings. *New Phytologist*, **119**, 69-81. https://doi.org/10.1111/j.1469-8137.1991.tb01009.x

[7] Yan, D., Wang, Z., Cheng, P., Chen, Y. and Zhang, Z. (2021) Rational Fabrication of Crystalline Smart Materials for Rapid Detection and Efficient Removal of Ozone. *Angewandte Chemie International Edition*, **60**, 6055-6060. https://doi.org/10.1002/anie.202015629

[8] Ignarro, L.J. (2014) Nitric Oxide. Reference Module in Biomedical Sciences. Elsevier, Amsterdam. https://doi.org/10.1016/B978-0-12-801238-3.00245-2

[9] Pilegaard, K. (2013) Processes Regulating Nitric Oxide Emissions from Soils. *Philosophical Transactions of the Royal Society B: Biological Sciences*, **368**, Article ID: 20130126. https://doi.org/10.1098/rstb.2013.0126

[10] Xiao, B., Wheatley, P.S. and Morris, R.E. (2007) The Adsorption, Storage and Release of Nitric Oxide Using Ion Exchanged Zeolites. *Studies in Surface Science and Catalysis*, **170**, 902-909. https://doi.org/10.1016/S0167-2991(07)80938-4

[11] Feng, X., Ding, X. and Jiang, D. (2012) Covalent Organic Frameworks. *Chemical Society Reviews*, **41**, 6010-6022. https://doi.org/10.1039/c2cs35157a

[12] Li, Z., *et al.* (2014) A 2D Azine-Linked Covalent Organic Framework for Gas Storage Applications. *Chemical Communications*, **50**, 13825-13828. https://doi.org/10.1039/C4CC05665E

[13] Rogge, S.M.J., *et al.* (2017) Metal-Organic and Covalent Organic Frameworks as Single-Site Catalysts. *Chemical Society Reviews*, **46**, 3134-3184. https://doi.org/10.1039/C7CS00033B

[14] Scicluna, M.C. and Vella-Zarb, L. (2020) Evolution of Nanocarrier Drug-Delivery Systems and Recent Advancements in Covalent Organic Framework-Drug Systems. *ACS Applied Nano Materials*, **3**, 3097-3115. https://doi.org/10.1021/acsanm.9b02603

[15] Liu, X., *et al.* (2019) Recent Advances in Covalent Organic Frameworks (COFs) as a Smart Sensing Material. *Chemical Society Reviews*, **48**, 5266-5302. https://doi.org/10.1039/C9CS00299E

[16] Ding, X., *et al.* (2011) Synthesis of Metallophthalocyanine Covalent Organic Frameworks That Exhibit High Carrier Mobility and Photoconductivity. *Angewandte Chemie International Edition*, **50**, 1289-1293. https://doi.org/10.1002/anie.201005919

[17] Xu, F., *et al.* (2015) Electrochemically Active, Crystalline, Mesoporous Covalent Organic Frameworks on Carbon Nanotubes for Synergistic Lithium-Ion Battery Energy Storage. *Scientific Reports*, **5**, Article No. 8225. https://doi.org/10.1038/srep08225

[18] Xu, H., Tao, S. and Jiang, D. (2016) Proton Conduction in Crystalline and Porous Covalent Organic Frameworks. *Nature Materials*, **15**, 722-726. https://doi.org/10.1038/nmat4611

[19] Zheng, Y., *et al.* (2021) Striped Covalent Organic Frameworks Modified Stationary Phase for Mixed Mode Chromatography. *Journal of Chromatography A*, **1649**, Article ID: 462186. https://doi.org/10.1016/j.chroma.2021.462186

[20] Song, Y., Sun, Q., Aguila, B. and Ma, S. (2019) Covalent Organic Frameworks: Opportunities of Covalent Organic Frameworks for Advanced Applications (Adv. Sci. 2/2019). *Advanced Science*, **6**, Article ID: 1970011. https://doi.org/10.1002/advs.201970011

[21] Jiang, H., Alezi, D. and Eddaoudi, M. (2021) A Reticular Chemistry Guide for the Design of Periodic Solids. *Nature Reviews Materials*, **6**, 466-487. https://doi.org/10.1038/s41578-021-00287-y

[22] Lohse, M.S. and Bein, T. (2018) Covalent Organic Frameworks: Structures, Synthesis, and Applications. *Advanced Functional Materials*, **28**, Article ID: 1705553. https://doi.org/10.1002/adfm.201705553

[23] Coôte, A.P., Benin, A.I., Ockwig, N.W., O'Keeffe, M., Matzger, A.J. and Yaghi, O.M. (2005) Porous, Crystalline, Covalent Organic Frameworks. *Science* (1979), **310**, 1166-1170. https://doi.org/10.1126/science.1120411

[24] El-Kaderi, H.M., *et al.* (2007) Designed Synthesis of 3D Covalent Organic Frameworks. *Science* (1979), **316**, 268-272. https://doi.org/10.1126/science.1139915

[25] Chen, L., Zhang, B., Chen, L., Liu, H., Hu, Y. and Qiao, S. (2022) Hydrogen-Bonded Organic Frameworks: Design, Applications, and Prospects. *Materials Advances*, **3**, 3680-3708. https://doi.org/10.1039/D1MA01173A

[26] Dash, B. (2018) Carbon Dioxide Capture Using Covalent Organic Frameworks (COFs) Type Material—A Theoretical Investigation. *Journal of Molecular Modeling*, **24**, 120-128. https://doi.org/10.1007/s00894-018-3646-3

[27] Frisch, M.J., *et al.* (2016) Gaussian 09, Revision A.02. Gaussian, Inc., Wallingford.

[28] Becke, A.D. (1993) Density-Functional Thermochemistry. III. The Role of Exact Exchange. *The Journal of Chemical Physics*, **98**, 5648-5652. https://doi.org/10.1063/1.464913

[29] Binkley, J.S., Pople, J.A. and Hehre, W.J. (1980) Self-Consistent Molecular Orbital Methods. 21. Small Split-Valence Basis Sets for First-Row Elements. *Journal of the American Chemical Society*, **102**, 939-947. https://doi.org/10.1021/ja00523a008

[30] Lu, T. and Chen, F. (2012) Multiwfn: A Multifunctional Wavefunction Analyzer. *Journal of Computational Chemistry*, **33**, 580-592. https://doi.org/10.1002/jcc.22885

[31] Humphrey, W., Dalke, A. and Schulten, K. (1996) VMD: Visual Molecular Dynamics. *Journal of Molecular Graphics*, **14**, 33-38. https://doi.org/10.1016/0263-7855(96)00018-5

[32] Ponnuchamy, V., Sandak, A. and Sandak, J. (2020) Multiscale Modelling Investigation of Wood Modification with Acetic Anhydride. *Physical Chemistry Chemical Physics*, **22**, 28448-28458. https://doi.org/10.1039/D0CP05165A